Diagnostics and Kinetic Modeling of a Hollow Cathode N_2O Discharge

T. de los Arcos, C. Domingo, V. J. Herrero, M. M. Sanz,† A. Schulz,‡ and I. Tanarro*

Instituto de Estructura de la Materia (CSIC), Serrano 123, 28006 Madrid, Spain

Received: April 7, 1998; In Final Form: May 13, 1998

The present work describes a systematic experimental investigation of a N_2O hollow cathode discharge. The local electron mean energy and density have been determined with a double Langmuir probe. Fourier transform infrared spectroscopy and mass spectrometry have been employed for the measurement of the concentration of the stable species present in the discharge. N_2O, N_2, O_2, and NO are always identified as the main constituents of the discharge plasma. In addition, NO_2 is found for the first time in a glow discharge of nitrous oxide. As a plausible explanation, a reaction of NO with oxygen atoms adsorbed on the cathode walls is proposed, although homogeneous reactions of vibrationally excited species cannot be discarded. A model based on a reduced set of kinetic equations including electron dissociation, gas-phase reactions, and gas−surface processes can give a global account of the measured data for all the experimental conditions used. The results are discussed and, when possible, compared to previous works on other types of N_2O glow discharges.

1. Introduction

Over the last two decades plasma processing has become a major technique in the electronic industry, where it is widely used for the etching and deposition of thin films of silicon and carbon compounds.[1] Cold plasmas are in principle more efficient than heat for the ionization and dissociation of the molecular precursors used in chemical vapor deposition (CVD) and provide in many cases an advantageous alternative to thermal CVD since a lowering of the deposition temperature diminishes an unwanted diffusion of dopants and the distortion of the substrate. The variation of the main parameters (discharge power and frequency, gas pressure and flux, substrate temperature) offers the possibility of changing the composition and properties of the deposited films. On the other hand, whereas the chemical reactions determining thermal CVD depend essentially on the substrate temperature and are reasonably well described with a thermodynamic formulation, plasma deposition is governed by a plethora of interrelated kinetic processes depending critically on small variations of the experimental conditions and for which basic data are often lacking. As a consequence, the knowledge of the plasma characteristics is in general limited and developments in the field are largely empirical.

One of the main products obtained by plasma-enhanced chemical vapor deposition (PECVD) is silicon dioxide, which finds widespread application as an interlayer dielectric for integrated circuits and in the fabrication of optical waveguides. SiO_2 has been deposited by PECVD mainly in radio frequency (rf) discharges of silane diluted in nitrous oxide. To get good quality films with rf discharges, substrate temperatures cannot be lower than 300−400 °C; at colder temperatures particle formation will negatively affect the properties of the deposited film. However, particle formation can be largely avoided, even with room-temperature substrates, by using low-frequency discharges.[2] Since nitrous oxide is usually the major constituent in the PECVD of silicon oxide, the systematic investigation of N_2O cold plasmas generated in low frequency or even direct current (dc) discharges can be of great help for the understanding of basic processes influencing the properties of SiO_2 thin films. In addition, nitrous oxide is also used in the deposition of other materials such as SiO_xN_y,[3] phosphosilicate glass layers,[4] and aluminum oxides.[5]

Glow discharges (GD), the usual procedure to generate cold plasmas,[1] not only are used in vapor deposition processes but find applications in many different fields such as spectroscopy[6] and kinetics[7] of unstable species, wall conditioning treatments in fusion devices,[8,9] or the decomposition of air pollutants.[10] Studies of various types of glow discharges containing nitrous oxide are documented in the literature. The diagnosis and modeling of rf discharges of pure N_2O have been reported by Cleland and Hess,[11,12] who used Fourier transform infrared spectroscopy (FTIR) for the determination of N_2O and NO, and by Kline et al.,[13] who employed downstream mass spectrometry for the monitoring of N_2O, NO, N_2, and O_2. O'Neil[14] has applied FTIR and diode laser IR spectroscopy for the study of vibrational excitation processes in this type of discharges. Microwave (MW) discharges of mixtures of N_2O with inert gases (Ar, N_2) are efficient sources of oxygen atoms, and their properties have also deserved attention. The O atom yields and, in some cases, the concentrations of atomic nitrogen or NO were determined by gas titration techniques.[15,16] Different kinetic schemes have been applied for the modeling of the various N_2O discharges just mentioned.

Another popular kind of glow discharges are those produced with hollow cathodes. Hollow cathodes provide a better geometric resolution of the different zones of the discharge and a better confinement of the plasma as compared with parallel plate electrodes and thus facilitate the use of diagnostic techniques for the investigation of basic plasma processes. As far as we know, no detailed studies of hollow cathode discharges

* Corresponding author.

† Present address: Departamento de Física Aplicada, Universidad Alfonso X el Sabio, Villanueva de la Cañada, 28691 Madrid, Spain.

‡ Present address: Alfred Wegener Institute for Polar and Marine Research, AWI, Research Department Potsdam, Telegrafenberg A43, 14473 Postdam, Germany.

S1089-5639(98)01749-6 CCC: $15.00
Published on Web 07/09/1998

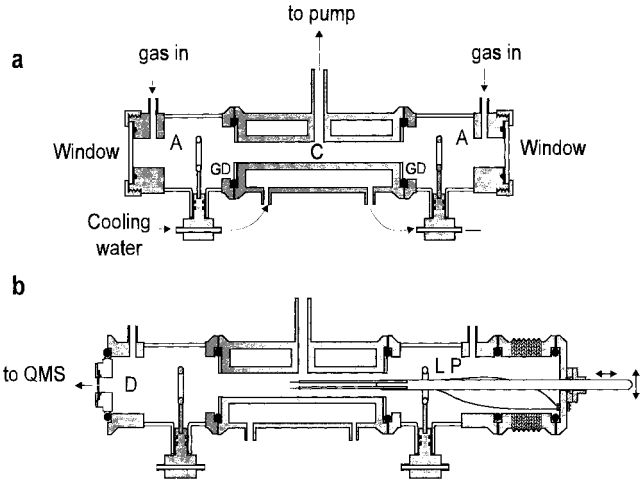

Figure 1. Schemes of the hollow cathode discharge cell as used (a) for FTIR absorption spectroscopy and (b) for mass spectrometry and for measurements with the double Langmuir probe. The meaning of the symbols is as follows: A, anode; C, hollow cathode; GD, glass disk; QMS, quadrupole mass spectrometer; LP, double Langmuir probe.

of N_2O have been published. In the present work we report the results of a systematic study of a N_2O hollow cathode dc discharge. To achieve a characterization as complete as possible of the nitrous oxide plasma, a combination of experimental techniques has been used. Electron energies and number densities were determined with a double Langmuir probe. FTIR spectroscopy was used for the monitorization of the nitrogen oxides NO and NO_2 produced in the discharge. As far as we know, this is the first observation of NO_2 in a nitrous oxide glow discharge. N_2 and O_2 were detected with a quadrupole mass spectrometer (QMS). The concentration of the N_2O precursor was determined with both, FTIR and QMS methods. The measurements were carried out for different gas flows through the discharge cell as well as for distinct values of both total pressure and discharge power. A kinetic model based on the numerical solution of the time-dependent differential equations for the relevant processes has been applied to the measurements. The results are discussed and compared to previous works.

2. Experimental Techniques

Hollow Cathode Discharge Cell. A scheme of the hollow cathode discharge cell used in this work is shown in Figure 1. It has been especially designed to be used for both mass spectrometry and FTIR absorption and emission spectroscopy, with a symmetrical, two-anode configuration, each one of them placed at each end of the hollow cathode, to ensure the uniformity and extension of the negative glow along the whole length of the cathode. The cylindrical stainless steel cathode is 90 mm long and has a 16 mm inner diameter. The two circular copper anodes, 16 mm inner diameter, are placed 25 mm from each end of the cathode. The total inner volume of the cell is 120 cm^3, and its total length 20 cm. The cathode and the copper bases of the anodes are refrigerated by water.

Two kinds of anode holders made of Pyrex and stainless steel can be used with different endings of the cell. One of them is designed to allocate either optical windows (F_2Ca) at each end of the cell for absorption spectroscopy, Figure 1a, or a window and a mirror for emission studies. The other kind of holder, Figure 1b, allows the allocation of a small diaphragm (80 μm diameter) in one side, to study the discharge by mass spectrometry, and of the Langmuir probe in the other one for electron energy and density measurements. The cathode and the anode holders can be easily connected or disassembled by means of 40 ISO-KF vacuum flanges. The cathode ends, in front of each anode, are covered with glass disks, 16 mm inner diameter, to prevent the extension of the negative glow outside the cathode. The cathode is grounded and each anode is connected, through an independent 5 KΩ ballast resistance, to the 2000 V, 150 mA high-voltage source. The independent connection allows the discharge to initiate simultaneously at both anodes. Current in the 10−70 mA range and voltages between 500 and 800 V have been employed in this work.

The discharge is sustained in a continuous flow of N_2O (Air Liquide, 99.5%), entering the reactor through two lateral tubes at the ends of the cell and being pumped out through the middle of the cathode. This ensures that all the N_2O passes through the plasma region and at the same time minimizes dirtiness by sputtering effects on the optical windows. The gas flow was measured by means of a calibrated rotameter and controlled by a needle valve placed at the entrance of the cell. The cell was evacuated by a rotary pump provided with a liquid nitrogen trap. The gas pressure in the cell was controlled with a regulating valve placed between the cell and the vacuum system and was measured by means of a capacitance manometer placed at the exit of the cathode (Leybold CM10, measurement range 10^{-3}−13 mbar). Corrections up to 15% were estimated for pressure readings at the highest fluxes because of the conductance of the tubular separation existing between the cell output and the manometer. In this study, flow rate varied between 3 and 265 sccm, at N_2O pressures (without discharge) between 0.5 and 2.5 mbar. Gas pressure increases by 10−15% when the discharge is turned on because of dissociation, especially for the lowest gas flow rates and the highest current values. This pressure growth increases slightly the conductance of the tubes and the regulating valve of the gas exit thus changing the effective pumping speed. The output gas flows correspond to an intermediate regime between laminar and molecular and the increase in conductance is found to be linear with the cell pressure, in accordance with model expectations.[17] The precise experimental calibration of this dependence and the estimate of its effect on the residence times included in the kinetic model, discussed below, have proved to be crucial in order to obtain suitable theoretical results. Without that correction, the model predicted a continuous increase of total pressure in the cell at the lowest gas flow values and did not reach a stationary state.

Langmuir Probe Measurements. Some attempts of using a single probe in order to measure the electron density in this work failed due to the appearance of a secondary glow discharge in the probe itself when its positive potential was increased above the plasma potential (some 400 V referenced to the cathode for a 2 mbar, 40 mA discharge), so it was not possible to reach the electron saturation current. To avoid this problem, ion density and mean electron energy were measured with a double Langmuir probe and a floating 50 Hz periodic potential between ±70 V. The $V-I$ characteristic curves were recorded on a digital oscilloscope connected through isolating electrical probes, working in the $X-Y$ mode. The experimental values were determined from probe data[18,19] by considering the electron energy distribution to be Maxwellian and assuming the standard orbit motion limited theory (OML). The double probe, Figure 1b, consisted of two 10 mm length, 65 μm radius tungsten wires, 1 mm apart, housed in two glass capillary tubes sealed at the end to define the beginning of the probe area.[20] It was mounted on a movable vacuum flange which allowed a ±1 cm displacement in the XY plane and some 10 cm displacement in the Z

axis. In this way, ion density and electron energy could be tested in different positions of the discharge, along the symmetry axis and along the cathode inner diameter. The measurements in the present work were fairly repetitive; neither metallic deposition by sputtering on the capillaries, which in some cases can increase the effective Langmuir probe area, nor heating probe effects, which sometimes cause electrical offsets, were observed.

FTIR Measurements. For the FTIR absorption measurements of the nitrogen oxides concentrations, a Bruker IFS66 spectrometer with both rapid-scan and step-scan options for the movable mirror was used. The spectral range of this apparatus was 400−7000 cm^{-1}. The step-scan option is specially suited for time-resolved FTIR spectroscopy and for the study of transients in the discharges.[21] In the present work the rapid-scan mode with a deuterated triglycine sulfate (DTGS) detector was used for the steady-state diagnostics of the N_2O discharge. The discharge cell is positioned within the sample chamber of the spectrometer, so that the infrared beam makes a single pass through its symmetry axis, being focused at the middle of the hollow cathode. The optical aperture of the instrument is selected in such a way that the width of the IR beam is always smaller than or equal to that of the negative glow region of the plasma, at any point of the cathode. A special arrangement was designed to accommodate the cell and allow dry air purging of the sample chamber and the optical bench, to prevent water vapor absorptions.

The maximum experimental resolution attainable with our FTIR spectrometer is 0.1 cm^{-1}, not enough to resolve the individual vib-rotational lines of the N_xO_y species. To determine the gas temperature and the N_xO_y species concentrations, a comparison with the simulated spectra of N_2O, NO, and NO_2 has been done by means of the spectroscopic data of wavenumbers and absorption coefficients of the HITRAN database.[22] These data have been treated in order to simulate a transmittance spectra, by taking into account optical path length effects (Lambert−Beer law), and assuming a Gaussian line shape for the natural line profiles. In the 0.5−2 mbar N_2O case, a Voigt profile would be more accurate than the Gaussian one, but in this case an independent experimental calibration at different N_2O pressures provided a good agreement with the results of the Gaussian simulation. An apodization function of the Blackman−Harris type with three terms, which supplies also a near Gaussian instrumental line shape, has been used in the FTIR spectrometer;[23] so, the simulated spectra have been convoluted with this instrumental line shape and converted into absorbance spectra for a direct comparison with the experimental results.

Mass Spectrometry Measurements. The measurement of N_2 and O_2 concentrations and an additional measurement of N_2O dissociation were made by means of mass spectrometry with a quadrupole mass spectrometer (QMS) Extrel, with electron impact ionization, and a secondary electron multiplier (channeltron) as detector, working in the current mode. Further details of its use for the study of hollow cathode discharges are given in previous publications.[24] This quadrupole was used to obtain the mass spectra of the discharge with the aid of a 1 V/μA preamplifier at the output of the channeltron and a digital Tektronix 2430A oscilloscope, working in the average mode. The quadrupole vacuum chamber was evacuated by means of a 300 l/s oil pump provided with a liquid nitrogen trap and backed by a 35 m^3/h rotary pump. A pressure of 7×10^{-7} mbar was achieved in the isolated chamber. The communication between the discharge cell and the quadrupole vacuum chamber was established by a gate valve and an aperture with a diameter of 80 μm located at the end of the cell. To obtain absolute concentration data, the sensitivity of the spectrometer to N_2 and N_2O was calibrated before and after each set of plasma measurements, by introducing these pure gases separately in the cell at various known pressures and measuring the instrumental response. Calibration of O_2 was usually made at the end of each set of measurements because even small amounts of O_2 can change slightly the conditions of the tungsten filament and shift temporally the efficiency of the whole spectrometer. In all three cases, linear dependencies of the QMS signal with pure gas pressures were obtained.

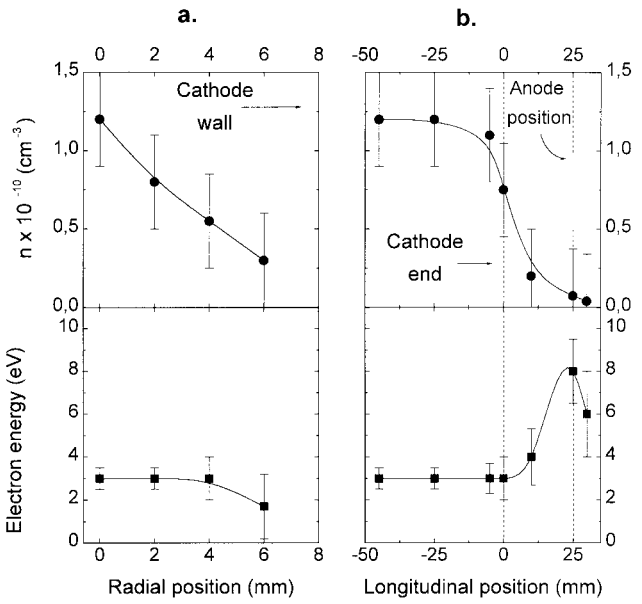

Figure 2. Experimental results of the geometrical distribution of the plasma parameters, obtained with the double Langmuir probe for a 40 mA, 2 mbar N_2O discharge. Ion number density (upper panel); electron energy (lower panel). The radial distribution inside the cathode is shown in (a) and the longitudinal distribution starting at the middle of the cathode and ending beyond the anode is shown in (b).

Precise NO measurements by means of mass spectrometry were precluded by the coincidence of its characteristic peaks in the mass spectrum with some peaks of the precursor N_2O. Moreover, the small concentrations of NO_2 detected by FTIR spectroscopy in our discharges could not be detected with the quadrupole, because a small but significative peak of N_2O appears also at the corresponding NO_2 charge/mass ratio, corresponding to heavier isotopes of N and O at their natural abundance.[25]

3. Experimental Results

Figure 2 shows the radial, Figure 2a, and longitudinal, Figure 2b, dependence of the ion density and mean electron energy. The data values for density and energy at each longitudinal position should be considered as a mean value along the length of the double probe (1 cm), especially at the edge of the cathode, where density values change markedly. In Figure 2b, corresponding to a 2 mbar, 40 mA, N_2O discharge, a constant value of both ion density (1.2×10^{10} cm^{-3}) and electron energy (2.8 eV) along the central cathode axis can be observed, while near the anode the ion density decreases noticeably and the electron energy increases up to ≈8 eV. Figure 2a shows an approximately linear decrease of ion density with the radius at a longitudinal fixed point near the middle of the cathode and a constant electron energy value, which only decreases slightly near the cathode wall. These results are in agreement with the general behavior of hollow cathode discharges.[1,26,27]

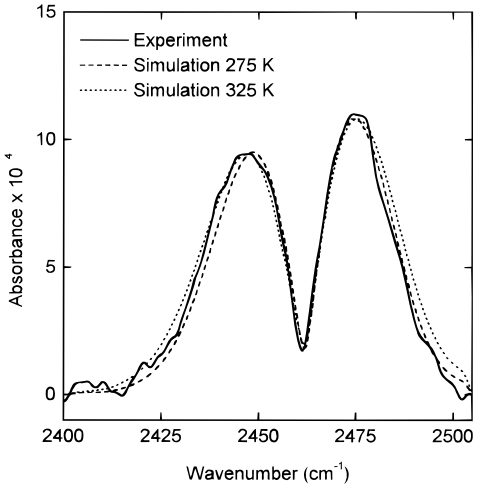

Figure 3. Experimental absorbance spectrum of the $\nu_1 + 2\nu_2$ band of N_2O with a 0.7 mbar initial N_2O pressure and a 40 mA discharge, and simulated spectra at 275 and 325 K.

The rotational temperatures and the extent of dissociation of the nitrous oxide in the hollow cathode discharge, as well as the rotational temperature and the absolute concentration of NO and NO_2 species produced in the process, were measured by FTIR absorption spectroscopy as indicated above. The NO_2 product could be detected in this work at a concentration 3 orders of magnitude lower than the precursor, because the strength, S, of its ν_3 band is 200 times higher than that employed for the N_2O measurements. Nevertheless NO_2 was not observed in N_2O microwave or rf discharges previously.[12,13,16]

A knowledge of the gas-phase temperature is necessary for estimating the concentrations of the gas-phase species and is important for the modeling of gas-phase reactions. Rotational and translational temperatures in the gas phase can be assumed to be in equilibrium under the present conditions. In fact, in previous works carried out in our laboratory,[28] both temperatures were measured to be in equilibrium in CH_4 hollow cathode discharges similar to this one by means of high-resolution IR laser spectroscopy. In that case Doppler broadening and line intensity relations led to the same temperature increase of the gas phase in the plasma, some 15 °C, above ambient temperature. The same kind of equilibrium behavior has been reported in rf glow discharges.[11,29,30] Figure 3 shows an experimental result of the $\nu_1 + 2\nu_2$ band of the N_2O spectrum at a resolution of 2 cm^{-1} with the discharge on (cathode and anodes refrigerated by water) and the simulated spectra at 275 and 325 K using the HITRAN data.[22] As can be seen, the temperature of the gas in the discharge does not increase above that of the water refrigerated cathode within this uncertainty in temperature values. Even spectra obtained without water refrigeration showed an increase of the gas temperature not higher than 50 °C, similar to that of the cathode wall.

For the study of temperature and concentration of the N_2O molecule, the $\nu_1 + 2\nu_2$ band system was used (2462 cm^{-1}, S = 7.25 cm^2 atm^{-1}). NO and NO_2 were studied by means of the fundamental (1876 cm^{-1}, S = 111 cm^2 atm^{-1}) and the ν_3 band systems (1617 cm^{-1}, S = 1446 cm^2 atm^{-1}), respectively. Absolute band intensities were taken from ref 31 and coincide with that of the HITRAN database. Figure 4 shows the N_2O spectrum of the cell without discharge (Figure 4a) and the spectrum with discharge on (Figure 4b). In this figure the appearance of NO and NO_2 can be observed. The inlet shows the corresponding decrease in N_2O absorbance.

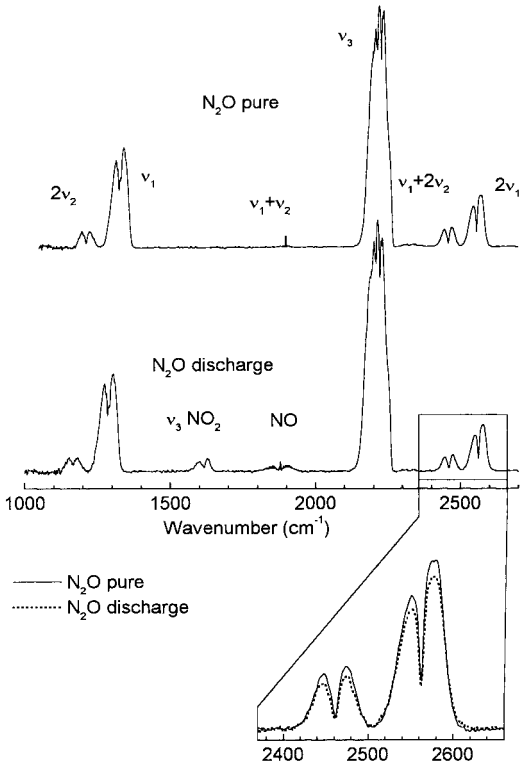

Figure 4. Spectrum of 1 mbar of N_2O in the cell (a) without discharge and (b) with discharge on (electrical current = 40 mA, flow rate = 3 sccm). The appearance of the fundamental band of NO and the ν_3 band of NO_2 and the decrease in the absorbance of the $2\nu_1$ and $\nu_1 + 2\nu_2$ bands of N_2O (inlet) during the discharge can be observed.

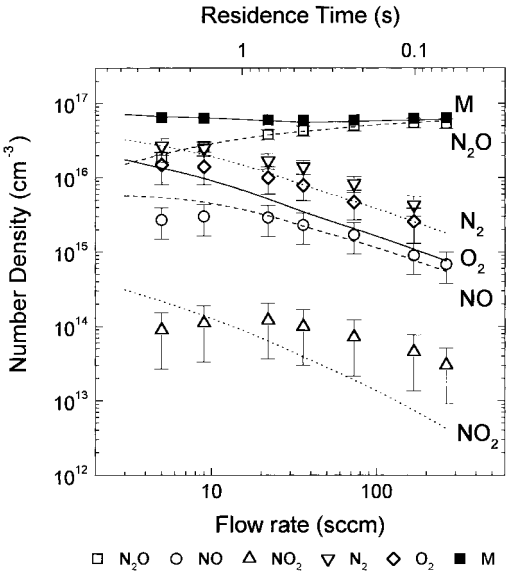

Figure 5. Experimental results (symbols) of the total number density (M) and of the number density of the various molecular species detected in a 40 mA, 2 mbar N_2O discharge at different flow rates. The measurements of the total (number density) concentration, M, were obtained with the capacitance manometer; those of the nitrogen oxides N_2O, NO, and NO_2 with FTIR absorption spectroscopy; and those of N_2 and O_2 by means of mass spectrometry. The N_2O concentrations were measured also with the quadrupole mass spectrometer and agreed with FTIR results within the respective experimental errors. The lines represent the predictions of the chemical kinetic model.

Figure 5 shows the experimental concentrations (symbols) for a 40 mA, 2 mbar N_2O discharge at different flow rates. The predictions of a kinetic model of the discharge (see below) are also represented (lines). The error bars shown in Figure 5 for

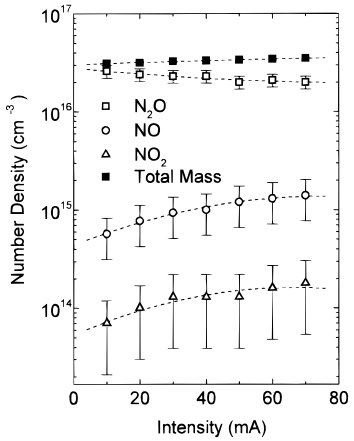

Figure 6. Experimental results of the dependence of the total number density (*M*) and the nitrogen oxides concentrations on electrical current, for a 1 mbar, 36 sccm N_2O discharge. The dashed lines have just been drawn through the data.

the FTIR measurements represent the 95% confidence interval obtained by considering a Student distribution for the statistical dispersion in the experimental measurements from different days (typically 4) for the same physical conditions of the discharge. Error bars for the mass spectrometric measurements account for the statistical dispersion in the experimental measurement of N_2 and O_2 concentrations as well as for the uncertainties in the respective calibrations. For the lowest concentrations obtained at the highest flow rates, where signals were smaller, the N_2 and O_2 error bars include also the contribution of the noise level. Error bars of the total concentration data, as measured with the capacitance manometer, are smaller than the size of the symbols.

As can be seen in Figure 5, the N_2O concentration decreases and those of N_2 and O_2 grow with decreasing gas flow input because the effects of electron impact dissociation are more marked for the longer residence times. The highest percentage of N_2O dissociation was ≈70%. Eventually, N_2 exceeds the precursor density at the lowest flow rate studied. On the other hand, the measured NO and NO_2 concentrations increase also with decreasing gas flow, but both species show a broad maximum at ≈20 sccm, and after that they decrease smoothly for the lowest N_2O flow rates. The total pressure grows slightly when flow rate decreases.

The results at 0.5 and 1 mbar N_2O starting pressure (not represented) show essentially the same behavior.

Figure 6 shows the effect of the electrical current on the concentration of nitrogen oxides present in the discharge. As expected, an increase in the current intensity leads to a larger dissociation of N_2O and to higher NO and NO_2 concentrations.

4. Chemical Kinetics Model and Discussion

To provide a better understanding of the kinetic processes involved in the discharge, a kinetic model has been developed in the present work and has been compared with our experimental results. The model is based on the numerical integration of a system of coupled differential equations accounting for the time evolution of the plasma species. In all cases, the integration is carried out until the steady state is reached. For the conditions of the present experiments this corresponds to times between ≈10 s for the slower flows and ≈1 s for the faster ones. The actual system of equations used for the simulation of the results has been obtained by a critical selection and adaptation to our experimental conditions of the kinetic equations considered in previous works on glow discharges (rf and MW) containing N_2O, as well as in the kinetic database of ref 32. The reactions finally included in the model after all trials and simplifications are shown in Table 1, and the model results for our experimental conditions are represented as lines in Figure 5. The relevant processes can be grouped into three kinds: electron dissociation of nitrous oxide, homogeneous gas-phase reactions involving atomic oxygen, and heterogeneous reactions. In the following we comment on each one of these types of processes.

TABLE 1: Reactions Included in the Kinetics Model of the N_2O Hollow Cathode Discharge. Rate Coefficients Are in Units of cm^3 molecule^{-1} s^{-1} for Dissociation by Electronic Impact and Bimolecular Reactions; cm^6 molecule^{-2} s^{-1} for Termolecular Reactions; and s^{-1} for Heterogeneous Reactions

reaction	rate constant	ref
Electron Impact Disocciation		
(1) $N_2O + e^- \rightarrow N_2 + O(^3P) + e^-$	7.8×10^{-10}	*a*
(2) $N_2O + e^- \rightarrow N_2 + O(^1D) + e^-$	3.2×10^{-10}	*a*
Neutral Gas-phase Reactions		
(3) $N_2O + O(^1D) \rightarrow 2\,NO$	7.2×10^{-11}	46
(4) $N_2O + O(^1D) \rightarrow N_2 + O_2$	4.8×10^{-11}	46
(5) $O(^1D) + N_2 \rightarrow O(^3P) + N_2$	2.0×10^{-11}	47
(6) $O(^1D) + NO \rightarrow O(^3P) + NO$	1.5×10^{-10}	39
(7) $O(^3P) + NO_2 \rightarrow NO + O_2$	9.5×10^{-12}	48
(8) $O(^3P) + NO + M \rightarrow NO_2 + M$	$(6.83-15.9) \times 10^{-32}$	36−38 (see text)
Heterogeneous Reactions		
(9) $O(^1D) + \text{wall} \rightarrow O(^3P)$	6140	*b*
(10) $O(^3P) + \text{wall} \rightarrow O(S)$	6140	*b*
(11) $O(^3P) + O(S) \rightarrow O_2$	26	12
(12) $NO + O(S) \rightarrow NO_2$	0.0009	*c*

[a] Estimated in this work. [b] Calculated for our cell geometry assuming $\gamma = 1$ in accordance with refs 12, 13 (see text). [c] Assumed in this work.

N_2O Dissociation. Electron impact dissociation of N_2O is the key process initiating the kinetics of the discharge. In the present work two N_2O electron dissociation channels have been considered, both producing $N_2 + O$, but with the oxygen atoms in its fundamental, ^3P, or in the excited, ^1D, state, respectively. The net disappearance of N_2O by electron impact dissociation depends on the plasma-to-reactor volume ratio (V_p/V_r), the electron density, n_e, and the sum of the respective rate constants for each dissociation channel for a given electron energy distribution. Consequently all of these quantities should be known for a correct modeling of the process.

In the present work, to avoid the inclusion of explicit dependencies of electron concentration on position, a uniform electron density distribution has been assumed throughout the plasma volume V_p inside the cathode, although the experimental results show a linear decrease of charge density with the distance to the cathode axis (Figure 2a). In this way, the mean value of $V_p \times n_e$ to be included in the differential equations is the result of the integral of $n_e \times dV_p$ along the entire cathode volume, obtained from the experimental measurements of the double Langmuir probe. In particular, a value $V_p \times n_e = 4.8 \times 10^{10}$ was obtained for the 2 mbar, 40 mA discharge selected to show the results of the model.

Experimental rate constants for electron impact dissociation at low energies are not available in general. They can be calculated, in principle, if the dependence of the cross sections with electron energy is well-known. Unfortunately, these cross sections are not available for most electron impact neutral dissociation reactions, especially in the low-energy range,[33] and on the other hand, the electron energy distribution in glow discharges, usually assumed to be Maxwellian, is not precisely

known. This lack of information prevents the rigorous calculation of the electron impact rate constants, and the values to be included in the model must be estimated by other means. In the present work the sum of the rate constants of the two ($k_1 + k_2$) N_2O electron impact dissociation channels was fitted in such a way that the predicted N_2O steady-state concentration, with discharge on, agreed with the experimental data. This rate constant sum value was estimated by neglecting, to a first approximation, the minor dissociation reaction of N_2O with neutral $O(^1D)$ also included in the model. With this approximation, the differential equation for the N_2O concentration can be expressed:

$$\frac{d[N_2O]}{dt} = \frac{\phi}{V_r} - \frac{[N_2O]}{\tau_{eff}}$$

which has the analytical solution of a pure exponential function and in the steady state leads to the value $[N_2O]_\infty = \phi\tau_{eff}$, where ϕ is the constant gas flow input and τ_{eff} ($\tau_{eff}^{-1} = \tau_d^{-1} + \tau^{-1}$) is the effective time constant for N_2O disappearance, which takes into account both dissociation ($\tau_d^{-1} = V_p n_e (k_1 + k_2)/V_r$) and removal by pumping (τ = residence time). This estimate was done for the highest gas flow value, where the assumption of negligible dissociation of N_2O by $O(^1D)$ is closest to reality, as it was verified afterward in the model (in any case, N_2O dissociation by $O(^1D)$ is always much less important that electron impact dissociation for all the conditions of the present work). In this way, a value $(k_1 + k_2) = 1.1 \times 10^{-9}$ cm^3 s^{-1} was obtained. As shown in Figure 5, this value can account in a nearly exact way for the percentage of N_2O dissociation over the whole range of gas flow conditions studied and also for the N_2 concentrations (reaction number 4 in Table 1, which is also a source of N_2, is at least 1 order of magnitude less significant than electron dissociation of N_2O). Moreover, modeling with this ($k_1 + k_2$) value agrees fairly well with the N_2O and N_2 experimental results obtained at other N_2O pressures, once the corresponding changes in electron densities, as measured with the double Langmuir probe, are taken into account.

The ratio between the k_1 and k_2 constants was selected in such a way that the predicted concentrations of NO fitted appropriately the experimental results. The calculated NO densities are particularly sensitive to this ratio, due to the very efficient channel of NO production by N_2O reaction with $O(^1D)$ atoms. On the contrary, the predicted N_2 and O_2 concentrations are almost insensitive to such variations. The values of k_1 and k_2 finally assumed were 7.8×10^{-10} cm^{-3} s^{-1} and 3.2×10^{-10} cm^{-3} s^{-1}, respectively, as listed in Table 1.

There are some discrepancies in the previous literature works on rf and microwave glow discharges of N_2O, concerning the possible N_2O electron impact dissociation pathways and their corresponding rate coefficients. These discrepancies reflect the lack of reliable information about the neutral dissociation cross sections involved in these processes.

Cleland and Hess[12] considered two dissociation channels: the reaction

$$N_2O + e^- \rightarrow N_2 + O(^3P) + e^-$$

included in Table 1, and the reaction

$$N_2O + e^- \rightarrow NO + N + e^- \qquad (13)$$

not included in the present model; their rate coefficients were assumed to change between $(0.32-2.20) \times 10^{-9}$ cm^{-3} s^{-1} and between $(0.35-2.40) \times 10^{-10}$ cm^{-3} s^{-1}, respectively, depending on the supplied rf power (5−20 W) and consequently on the reported mean electron energy (3−6 eV). Although these rate constants were obtained just by fitting the experimental results, the authors made a theoretical estimate assuming a Maxwell (and a Druyvesteyn[1]) electron energy distribution and approximating the cross section as a step function. From this estimate the authors justified the fact that the rate coefficient for the second reaction is nearly 10 times smaller than that of the first one because of the different threshold energies (1.67 and 4.93 eV) of the respective dissociation channels.[34] However, in their case the k values fitted from the experimental measurements were systematically almost 1 order of magnitude lower than the theoretically estimated ones. On the other hand, Cleland and Hess omitted reaction 2 of Table 1, but included instead the excitation of the $O(^3P)$ atoms by electron impact, to produce the $O(^1D)$ atoms responsible in part for the appearance of NO (reaction 3 of Table 1).

On the contrary, Kline et al.[13] included dissociation reactions 1 and 2 of Table 1 but omitted in their model reaction 13, arguing that the N and NO produced in this reaction react very rapidly to produce N_2 and $O(^3P)$ through the homogeneous reaction

$$N + NO \rightarrow N_2 + O(^3P) \qquad k = 3.0 \times 10^{-11}\ \text{cm}^{-3}\ \text{s}^{-1} \quad (14)$$

in such a way that both reactions compensate each other. The same behavior was assumed by Ung.[15] The compensation of eqs 13 and 14 was corroborated by Cleland and Hess,[12] who considered both reactions explicitly, and was also observed by us when reactions 13 and 14 were included in our kinetic model. Consequently these two reactions, which could be considered as intermediate steps of reaction 1 In Table 1, have been also omitted in our case.

Kline et al.[13] estimated the electron energy distribution by means of a Monte Carlo calculation, determining the rate coefficients for neutral N_2O dissociation by electronic impact from photodissociation data at high VUV photon energies (8−11 eV).[35] Therefore the energy values considered in this reference seem to be remarkably higher than those found in the present work from Langmuir probe data. Consequently, they assumed the rate coefficient to be $k_1 = 5.4 \times 10^{-9}$ cm^{-3} s^{-1}, much larger than the highest value assumed by Cleland and Hess (at 6 eV mean electron energy), and $k_2 = 6.75 \times 10^{-10}$ cm^{-3} s^{-1}. On the other hand, Piper et al.[16] in N_2O/Ar, MW discharges found a better agreement between their experimental and modeling results assuming reaction 1 to be the only dissociation channel and neglecting reaction 2, while Ung[15] assumed both reactions to be significant in N_2O/N_2 discharges. In these two last cases, Ar and N_2 effects on the kinetics of the processes were included, respectively. None of these authors gave information about their electron energy distributions.

In our case, the rate constant value assumed for the first reaction is of the same order as that used by Cleland and Hess[12] for their lowest electron energy distribution, with a mean electron energy ≈3 eV, and the rate constant for the second reaction is lower than half the value assumed for the first reaction, its threshold energy being approximately twice that of the first reaction (3.62 eV).[34]

Another significant difference between the work of Kline et al.[13] and the former works[12,16] is the inclusion in the model of Kline et al. of the dissociation by electronic impact of the predominant reaction products, NO, N_2, and O_2, as well as the consideration of ionization and dissociative ionization channels for these products and for N_2O. Nevertheless the rate constants estimated by these authors were 10 or more times smaller than

those for neutral dissociation and did not influence significantly their model predictions. Although high-energy electrons in the tail of the electron energy distribution are known to be responsible for sustaining the discharge, in the present work these reactions have not been included in the kinetic model, given the experimental mean electron energy of 3 eV, the considerably higher bond strengths of the diatomic products (N_2 = 9.76 eV, O_2 = 5.11 eV, NO = 6.5 eV) and the even higher ionization threshold energies (N_2O = 12.89 eV; NO = 9.26 eV, N_2 = 15.58 eV, O_2 = 12.07 eV).[33] In fact, experiments with hollow cathode discharges of N_2 and O_2 carried out in our laboratory did not show appreciable dissociation of these molecules.

Homogeneous Reactions. Rate coefficients for the binary neutral homogeneous reactions involving oxygen atoms (3−7) shown in Table 1 are assumed to be the same as those of refs 12 and 13, their original bibliographic source being cited in the fourth column of this table. A general agreement was found among these values and the values compiled in ref 32 and references therein for temperatures of 300 K. The three-body rate coefficient taken into account for reaction 8 has been considered at each moment of the simulation to depend on the relative concentration of the predominant species N_2O, N_2, and O_2 and their partial contribution as a third body. The individual values used here have been 1.59×10^{-31} cm^{-6} s^{-1},[36] 6.83×10^{-32} cm^{-6} s^{-1},[37] and 8.6×10^{-32} cm^{-6} s^{-1},[38] respectively. These reactions are assumed to be irreversible, this assumption being justified by comparison of the reverse and forward rate constants.[39,40] Homogeneous reactions among two or three of the stable species involved in the discharge have not been considered in the model, since their reported rate coefficients are many orders of magnitude lower than those of reactions involving atoms.

Vibrational temperatures in N_2O glow discharges are known to be hotter than the translational and rotational ones;[14] however, reactions of vibrationally excited species have not been considered in previous modelings of rf discharges of nitrous oxide.[12,13] We have also taken this view, but a word of caution is needed at this point. The efficiency of vibrational excitation could be larger in dc than in rf glow discharges having a similar mean electron energy at the center of the plasma, due to the higher energy electrons present in the anode fall region of dc discharges.[1] As a consequence, reactions of vibrationally excited molecules might play a more significant role in the present hollow cathode discharge than in the previous rf experiments. In particular, reactions of vibrationally excited nitrogen oxides could be the cause of the small but appreciable NO_2 concentration found in our experiments and not present in the former rf studies.[12,13] Although this possibility of NO_2 production cannot be ruled out, in the absence of more direct evidence, reactions of vibrationally excited molecules have not been included in the model due to the uncertainty about the actual processes to be considered and to the scarcity of literature data on the relevant cross sections. Instead of that, a wall reaction is proposed as the main source of NO_2.

Heterogeneous Reactions. The heterogeneous reactions (9−12) considered in the present work contribute slightly to the deexcitation of the O(^{1}D) atoms and represent efficient channels of O(^{3}P) disappearance and O_2 formation and a source for NO_2. This contribution to O_2 and NO_2 production is achieved by reaction of O(^{3}P) and NO, respectively, with the oxygen atoms adsorbed previously in the wall, O(S). The wall recombination of oxygen atoms to yield O_2 has been also considered relevant in the previous works on N_2O rf discharges.[12,13] In our model, this mechanism is the main channel of O_2 production. For lack of a better hypothesis, a single heterogeneous reaction of NO with O(s) has been assumed, to account approximately for the observed concentration of NO_2, while keeping the model as simple as possible. It should be recalled here that no NO_2 was detected in the previous studies of N_2O glow discharges reported in the literature.[12,13,15,16] The wall reaction of NO was incorporated once the homogeneous reactions included were seen to be insufficient to explain the NO_2 balance and after the rest of the homogeneous reactions of nitrogen oxides described in the literature, which could contribute to NO_2 production, were discarded because of their very small rate coefficients. In particular the well-known reaction $2NO + O_2 \rightarrow 2NO_2$ has a room-temperature rate constant of $\approx 2 \times 10^{-38}$ cm^{-3} s^{-1}.[41]

The rate coefficients assumed for the heterogeneous reactions were estimated by taking into account the probability per individual collision, γ_x, of deexcitation, sticking, or reaction of each species X with the wall, and the frequency of wall collisions, which is related to the mean velocity ϖ_x, the concentration [X], and the active surface/volume ratio of the reactor, through the expression[12,42]

$$K_{x,wall}[X]V_x = [X]\varpi_x\gamma_x A/4$$

where A is the reactive wall area and V_x the volume occupied by the X species. A value of $\gamma_x = 1$ was assumed for O(^{1}D) deexcitation and for O(^{3}P) sticking on stainless steel, in agreement with previous works.[12,13] The value for the fraction of O(^{3}P) wall collisions on stainless steel that result in recombination is 0.0042[12] at 300 K. O(^{3}P) sticking on the Pyrex anode holders was not included after verifying its negligible effect on the model calculations, due to its small sticking coefficient $\gamma = 4 \times 10^{-4}$ as compared with stainless steel.[43]

In the literature, there are some hints of wall processes converting NO to NO_2,[44] and although the proposed mechanisms are inconclusive, they do not include a direct reaction of NO molecules with adsorbed atomic oxygen, since these studies do not pertain to discharges or dissociation processes that would yield oxygen atoms. To the best of our knowledge no rate constants for the wall reaction of NO included in the model are available. In the present work the γ value for NO_2 formation by reaction of NO with oxygen atoms adsorbed on the cathode, O(S), has been assumed to be 2×10^{-7}. This very small value of γ is enough to justify approximately the experimental NO_2 concentration observed in our discharge cell. The heterogeneous rate coefficients obtained with the different γ_x values are shown in Table 1.

The rate coefficients assumed for the reactions 9 and 10 in the model by wall recombination and geometrical considerations are slightly smaller than those that would correspond to the diffusion-limited case, $k_d = D/\Lambda^2$,[45] with D the diffusion coefficient and Λ the characteristic diffusion length ($k_d \sim 8000$). This fact indicates that O atoms diffuse slightly faster than they recombine in the walls, so the k_9 and k_{10} values given in Table 1 have not been changed. On the other hand, the rate coefficients for reactions 11 and 12 are some orders of magnitude smaller than those estimated from the diffusion limit.

Differential Equations. Table 2 shows the set of coupled differential equations obtained from the reactions included in Table 1. It has been numerically solved by means of a fourth-order Runge−Kutta method. The solution of this set of equations yields the time evolution of the concentrations of each species from the beginning of the discharge to the attainment of the stationary state. In the present work only the steady-

TABLE 2: Set of Coupled Differential Equations Obtained from the Reactions Included in Table 1. ϕ_{N_2O} Is the Flow Rate of N_2O into the Reactor in Molecules s^{-1}, V_R is the Reactor Volume (cm^3), V_C the Cathode Volume (cm^3), S_C the Cathode Surface (cm^2), and τ the Reactor Residence Time (s^1)

$$V_R\frac{d[N_2O]}{dt} = \Phi_{N_2O} - (k_1 + k_2)[N_2O][e^-]V_P - (k_3 + k_4)[N_2O][O(^1D)]V_C - [N_2O](V_R/\tau)$$

$$V_R\frac{d[NO]}{dt} = 2k_3\,[N_2O][O(^1D)]V_C - k_8[NO][O(^3P)][M]V_R + k_7[NO_2][O(^3P)]V_R - k_{12}[NO][O(S)]V_RS_C - [NO](V_R/\tau)$$

$$V_R\frac{d[N_2]}{dt} = (k_1 + k_2)[N_2O][e^-]V_P + k_4[N_2O][O(^1D)]V_C - [N_2](V_R/\tau)$$

$$V_R\frac{d[O_2]}{dt} = k_4[N_2O][O(^1D)]V_C + k_7[NO_2][O(^3P)]V_R + k_{11}[O(^3P)][O(S)]V_RS_C - [O_2](V_R/\tau)$$

$$V_R\frac{d[NO_2]}{dt} = k_8[NO][O(^3P)][M]V_R - k_7[NO_2][O(^3P)]V_R + k_{12}[NO][O(S)]V_RS_C - [NO_2](V_R/\tau)$$

$$V_C\frac{d[O(^1D)]}{dt} = k_2[N_2O][e^-]V_P - (k_3 + k_4)[N_2O][O(^1D)]V_C - k_5[N_2][O(^1D)]V_C - k_6[NO][O(^1D)]V_C - k_9[O(^1D)]V_C$$

$$V_R\frac{d[O(^3P)]}{dt} = k_1[N_2O][e^-]V_P + k_5[N_2][O(^1D)]V_C + k_6[NO][O(^1D)]V_C - k_8[NO][O(^3P)][M]V_R - k_7[NO_2][O(^3P)]V_R + k_9[O(^1D)]V_C - k_{10}[O(^3P)]V_C - k_{11}[O(^3P)][O(S)]V_RS_C$$

$$S_C\frac{d[O(S)]}{dt} = k_{10}[O(^3P)]V_C - k_{11}[O(^3P)][O(S)]V_RS_C - k_{12}[NO][O(S)]V_RS_C$$

state predictions of the model are compared with the experimental results, but the study of the transient behavior is also in progress.[21]

Besides the five stable molecular species N_2O, N_2, O_2, NO, and NO_2 and the oxygen atoms appearing in the gas phase or adsorbed on the cathode wall, the model takes into account the overall mass balance, *M*, in such a way that the sum of concentrations of all the species equals that predicted by the ideal gas law and allows the estimation of the total pressure in the reactor. The pressure variation in the discharge cell determines the variation in the output conductances of the experimental system, which were previously calibrated with pure N_2O for different pressures and flow rates. This dependence had to be incorporated into the model for the precise estimation of residence times (τ_p), because it influences very remarkably the process of removal by pumping of each stable species, especially at low flow rates. On the contrary, since the rates at which $O(^1D)$ and $O(^3P)$ disappear by heterogeneous recombination and gas-phase reactions are many times larger than the rate at which they are pumped, the inclusion of a pumping term in the two differential equations for these oxygen atoms has been verified to be irrelevant.

In the present model, the reaction volume for all the molecular species involved in the process was assumed to be the whole cell volume, so the assumption that the reagents are well mixed is included implicitly. To evaluate this assumption, the characteristic diffusion time $\tau_d = k_d^{-1}$ of each species in N_2O has been estimated.[45] In our case, with 2 mbar of N_2O in the hollow cathode discharge cell, one gets $\tau_D \approx 2$ ms for N_2O diffusion and even smaller values for the lighter diatomic products and the oxygen atoms. This characteristic τ_d is smaller in any case than the residence times ($\tau \approx 47$ ms to 4.7 s) for all the gas flows rates studied ($\phi = 3-300$ sccm), so diffusive transport dominates over convection by pumping, and the reactor can be considered effectively well mixed.

The $O(^1D)$ atoms are deexcited very fast by collisions with N_2O and other stable species through reactions 3−6, with typical deexcitation times of some microseconds, considerably smaller than their diffusion time; therefore the reaction volume for this species has been assumed to be that of the cathode. On the contrary, the disappearance of $O(^3P)$ by homogeneous or heterogeneous reactions has characteristic times in the millisecond range, and an effective volume equal to that of the reactor has been considered.

Model Results. In Figure 5 the results of the chemical kinetic model are compared with the experimental measurements. It should be taken into account that the results of the calculations are affected by a series of error sources, even assuming that the kinetic model and the temporal and geometrical approximations included are all right. These uncertainties have not been estimated explicitly but could be ascribed to errors in the input data such as the rate constants found in the literature or assumed in the model, in the precise experimental determination of the temperature of the neutrals, in the dependence of the residence time with total pressure, etc.

The experimental total pressure and the extent of N_2O dissociation are accounted for very well by the chemical kinetic model for all the flow rates investigated; furthermore, there is an encouraging agreement between the measured N_2, O_2, and NO concentrations and the theoretical results. The order of magnitude of the NO_2 concentrations can be approximately reproduced with the assumed NO wall reaction parameter, although the model predictions yield a steeper decay of NO_2 concentration with increasing flow rate than that observed experimentally. The $O(^3P)$ atom concentrations predicted by the model, not shown in the figure, decrease slightly with flow rate and are always lower than 2×10^{12} cm^{-3}, and $O(^1D)$ atom concentrations are considerably smaller.

The application of the present model to the rf and MW N_2O discharges previously reported in the literature is not easy, even in the cases when the mean cathode electron energies and the residence times are similar. The problems appear mainly because relevant experimental conditions, especially the surface properties of the electrodes and the walls of the respective reactors, can be very different, and their effects on the species attributed in the model to heterogeneous reactions and thus on

NO_2 and O_2 production are difficult to estimate. In fact, as indicated above, NO_2 has not been observed previously in N_2O discharges. For the species whose concentrations are determined by homogeneous reactions, a comparison is more meaningful. We have applied the present chemical kinetic model to the rf N_2O glow discharge studied by Cleland and Hess.[12] The N_2O and NO FTIR experimental data of their 5 W, 40 sccm discharge, with a reported mean electron energy very similar to that of the present work, were analyzed with our model. The agreement found between our results and their experimental data is encouraging: The calculated steady-state mole fractions are 0.6 for N_2O and 0.06 for NO, as compared with their experimental values of 0.75 ± 0.1 and 0.03 ± 0.02, respectively (see Figure 6 of ref 12).

5. Summary and Conclusions

In this work a hollow cathode dc discharge of N_2O has been studied for the first time. FTIR absorption spectroscopy and mass spectrometry have been employed for the determination of the absolute concentration of the stable neutral species and a double Langmuir probe has been used for the measurement of the average local electron energy and ion density within the plasma. The temperature of the nitrogen oxides present in the discharge was derived from an analysis of the IR band contours. This combination of experimental techniques and the better confinement of the plasma achieved in the hollow cathode discharge has allowed a more complete characterization of the relevant kinetic processes than that reported in former investigations of N_2O glow discharges.

In accordance with previous studies on these type of discharges, N_2O, N_2, O_2, and NO are the predominant species in the plasma. Under our experimental conditions NO contributes always less than 10% to the total number density. In addition, a small amount of NO_2 has been clearly identified, for the first time to our knowledge, in a glow N_2O discharge. The concentration of this last species is typically more than an order of magnitude smaller than that of NO.

To rationalize the collected set of data, a simple chemical kinetics model including a reduced number of reactions is proposed. The corresponding set of coupled, time-dependent, differential equations has been numerically solved, and the steady-state solutions have been compared with the measurements. The agreement between the model predictions and the experimental data for the N_2O, N_2, O_2, and NO is good. The calculations can also reproduce the order of magnitude of the NO_2 concentration.

According to the model results, the concentrations of N_2O and N_2 are essentially determined by electron impact dissociation and that of NO, mainly by gas-phase reactions. The amount of molecular oxygen is regulated partly by wall recombination of oxygen atoms and partly by gas-phase processes. The small, but detectable quantity of NO_2 is attributed mainly to a heterogeneous wall reaction. Homogeneous reactions of vibrationally excited species could provide an alternative explanation for the appearance of NO_2; however, this possibility has not been explored in the present model.

The rate constants for the gas-phase reactions have been taken directly from current kinetic databases, and the coefficients for the electron dissociation of N_2O are similar to those of previous glow discharge works with a similar electron energy. A considerable effort has been devoted to the identification of the possible sources of NO_2 in the discharge cell, since the reactions contemplated in the available kinetic models published in the literature predict, for the present hollow cathode cell, NO_2 concentrations several orders of magnitude lower than those actually observed. After an unsuccessful search of plausible gas-phase mechanisms of NO_2 production, a single heterogeneous reaction of NO with oxygen atoms adsorbed in the cathode wall is proposed tentatively as a likely explanation. A rate coefficient implying a small probability for this wall reaction was enough to reproduce globally the experimental NO_2 concentration. The present results indicate that the possible presence of NO_2 in glow discharges of nitrous oxide should be considered in the analysis of more complex plasmas, like those used for the deposition of silicon compounds.

The general agreement between calculations and experiment suggests that the model provides a reasonable global description of the processes performed on the hollow cathode N_2O discharge. At present, a truly accurate modeling of glow discharges is hampered by a lack of basic data, most notably rate constants for low-energy electron dissociation and surface reactions. The experimental investigation of these phenomena is in general complex and poses important technical problems. However much insight could still be gained from a further study of gas-phase processes. In this respect the direct monitoring of the atomic concentrations, the study of the molecular excited states by emission spectroscopy, or the experimental investigation of the stable species during the transient time before the attainment of the steady-state condition would certainly provide most valuable information.

Acknowledgment. We are indebted to J. L. Domenech, who wrote the program for the simulation of the spectra, and to F. L. Tabarés for his careful reading of the manuscript. The technical advice and support of J. M. Castillo, M. A. Moreno, and J. Rodríguez have been most valuable for the achievement of the present experiments. The DGICYT of Spain (Projects PB94-128, PB95-0918-C03-02) and the Comunidad de Madrid (Project COR0031/94), as well as the EC (Contract ERBCH-BGCT940551 and Project PL950099) are gratefully acknowledged for financial support.

References and Notes

(1) Grill, A. *Cold Plasma in Materials Fabrication*; IEEE Press: New York, 1994.

(2) Yamaguchi, T.; Sakamoto, N.; Shimozuma, M.; Yoshino, M.; Tagashira, H. *J. Appl. Phys.* **1998**, ***83***, 554.

(3) Lam, D. K. W. *Appl. Opt.* **1984**, *23*, 2744.

(4) Takamatsu, A.; Shibata, M.; Sakai, H.; Yoshimi, T. *J. Electrochem. Soc.* **1982**, *131*, 1865.

(5) Kim, Y.-C.; Chun, J. S.; Lee, W.-J. *Thin Solid Films* **1995**, *258*, 67.

(6) Tanarro, I.; Sanz, M. M.; Domingo, C.; Bermejo, D.; Santos, J.; Domenech, J. L. *J. Phys. Chem.* **1994**, *98*, 5862.

(7) Shved, G. M.; Khvorostovskaya, L. E.; Potekhin, I. Yu.; Demyanikov, A. I.; Kutepov, A. A.; Fomichev, V. I. *Izv. Acad. Nauk. SSSR Atmos. Oceanic Phys.* **1991,** *27*, 295.

(8) Sasaki, Y. T. *J. Vac. Sci. Technol.* **1991**, *A9*, 2025.

(9) Tabarés, F. L.; Tafalla, D. *J. Vac. Sci. Technol. A* **1996**, *14*, 3087.

(10) Penetrante, B. M.; Hsiao, M. C.; Bardsley, J. N.; Merritt, B. T.; Vogtlin, G. E.; Kuthi, A.; Burkhart, C. P.; Bayless, J. R. *Plasma Sources Sci. Technol.* **1997**, *6*, 251.

(11) Cleland, T. A.; Hess, D. W. *J. Appl. Phys.* **1988**, *64*, 1068.

(12) Cleland, T. A.; Hess D. W. *J. Electrochem. Soc.* **1989**, *136*, 3103.

(13) Kline, L. E.; Partlow, W. D.; Young, R. M.; Mitchell, R. R.; Congedo, T. V. *IEEE Trans. Plasma Sci.* **1991**, *19*, 278.

(14) O'Neil, J. A. *J. Vac. Sci. Technol.* **1991**, A9, 669.

(15) Ung, A. Y. M. *Chem. Phys. Lett.* **1975**, *32*, 351.

(16) Piper, L. G.; Rawlins, W. T. *J. Phys. Chem.* **1986**, *90*, 321.

(17) Roth, A. *Vacuum Technology*; North-Holland: New York, 1982.

(18) Schott, L. Electrical Probes. In *Plasma Diagnostics*; Lochte-Holtgreven, W., Ed.; AIP Press: New York, 1995; Chapter 11.

(19) Cox, I.; et al. *J. Phys. D: Appl. Phys.* **1987**, *20*, 820.

(20) Felts, J.; Lopata, E. *J. Vac. Sci. Technol.* **1987**, *A5*, 2274.

(21) (a) Domingo, C.; de los Arcos, T.; Tanarro, I.; Sanz, M. M. *SPIE* **1997**, *3090*, 308. (b) To be published.
(22) Rothman, L. S. *J. Quant. Spectrosc. Radiat. Transfer* **1992**, *48*, 469.
(23) Harris, F. J. *Proc. IEEE* **1978**, *66*, 51.
(24) Sanz, M. M.; Abad, L.; Herrero, V. J.; Tanarro I. *J. Appl. Phys.* **1992**, *71*, 5372.
(25) *Eight Peak Index of Mass Spectra*; The Royal Society of Chemistry, 1985.
(26) Mavrodineau, R. *J. Res. Nat. Bur. Standards* **1984**, *89*, 143.
(27) Bukvic, S.; Labat, J. M. *Phys. Scr.* **1992**, *46*, 57.
(28) Tanarro, I.; Sanz, M. M.; Bermejo, D.; Domingo, C.; Santos, J. *J. Chem. Phys.* **1994**, *100*, 238.
(29) Davis, G. P.; Gottscho, R. A. *J. Appl. Phys.* **1983**, *54*, 3080.
(30) Farrow, L. A. *J. Chem. Phys.* **1985**, *82*, 3625.
(31) Smith, M. A. H.; Rinsland, C. P.; Fridovich, B.; Rao, K. N. Intensities and collision broadening parameters for infrared spectra. In *Molecular Spectroscopy: Modern Research*; Rao, K. N., Weber, A., Eds.; Academic Press: San Diego, 1985; Vol. III.
(32) *NIST Chemical Kinetics Database, Version 4.0*; U.S. Department of Commerce: Gaithersburg, 1992.
(33) *Database Needs for Modeling and Simulation of Plasma Processing*; Nat. Res. Council, National Academy Press: Washington, DC, 1996.
(34) Radzig, A. A.; Smirnov, B. M. *Reference data of Atoms, Molecules and Ions*; Springer-Verlag: Berlin, 1980.
(35) Black, G.; Sharpless, R. L.; Slanger, T. G.; Lorents, D. C. *J. Chem. Phys.* **1975**, *62*, 4266.
(36) Furuyama, S.; Atkinson, R.; Colussi, A. J.; Cvetanovic, R. J. *Int. J. Chem. Kinet.* **1974**, *6*, 741.
(37) Roscoe, J. M. *Can. J. Chem.* **1988**, *66*, 2325.
(38) Atkinson, R.; Baulch, D. L.; Cox, R. A.; Hampson, R. F., Jr.; Kerr, J. A.; Troe J. *J. Phys. Chem. Ref. Data* **1989**, *18*, 881.
(39) McEwan, M. J.; Phillips L. F. *Chemistry of the Atmosphere*; John Wiley and Sons: New York, 1975.
(40) Chase, M. W., Davies, C. A., Downey, J. R., Frurip, D. J., McDonaald, R. A., Syverud, A. N., Eds. *JANAF Thermochemical Tables*, 3rd ed.; U.S. National Bureau of Standards: Washington, DC, 1985.
(41) Olbregts, J. *Int. J. Chem. Kinet.* **1985**, *17*, 835.
(42) Sabadil, H.; Pfau, S. *Plasma Chem. Plasma Process.* **1985**, *5*, 67.
(43) Brake, M. L.; Kerber, R. L. *Plasma Chem. Plasma Process.* **1983**, *3*, 79.
(44) Heicklen, J.; Cohen, N. *Adv. Photochem.* **1968**, *5*, 157.
(45) Chantry, P. J. *J. Appl. Phys.* **1987**, *62*, 1141.
(46) Lam, L.; Hastie, D.; Ridley, B. A.; Schiff, H. I. *J. Photochem.* **1981**, *15*, 119.
(47) Schofield, K. *J. Photochem.* **1978**, *9*, 55.
(48) Baluch, D. L.; Drysdale, D. D.; Horne, D. G.; Lloyd A. C. *Evaluated Kinetic Data for High-Temperature Reaction: II. Homogeneous Gas-Phase Reactions of the H_2-N_2-O_2 System*; Butterworth: London, 1973.